

The $b\bar{b}$ Production Cross Section and Angular Correlations in $p\bar{p}$ Collisions at $\sqrt{s} = 1.8$ TeV

B. Abbott,⁴⁸ M. Abolins,⁴⁵ V. Abramov,²¹ B.S. Acharya,¹⁵ D.L. Adams,⁵⁵ M. Adams,³²
V. Akimov,¹⁹ G.A. Alves,² N. Amos,⁴⁴ E.W. Anderson,³⁷ M.M. Baarmand,⁵⁰
V.V. Babintsev,²¹ L. Babukhadia,⁵⁰ A. Baden,⁴¹ B. Baldin,³¹ S. Banerjee,¹⁵ J. Bantly,⁵⁴
E. Barberis,²⁴ P. Baringer,³⁸ J.F. Bartlett,³¹ U. Bassler,¹¹ A. Bean,³⁸ A. Belyaev,²⁰
S.B. Beri,¹³ G. Bernardi,¹¹ I. Bertram,²² V.A. Bezzubov,²¹ P.C. Bhat,³¹ V. Bhatnagar,¹³
M. Bhattacharjee,⁵⁰ G. Blazey,³³ S. Blessing,²⁹ A. Boehnlein,³¹ N.I. Bojko,²¹
F. Borchering,³¹ A. Brandt,⁵⁵ R. Breedon,²⁵ G. Briskin,⁵⁴ R. Brock,⁴⁵ G. Brooijmans,³¹
A. Bross,³¹ D. Buchholz,³⁴ M. Buehler,³² V. Buescher,⁴⁹ V.S. Burtovoi,²¹ J.M. Butler,⁴²
F. Canelli,⁴⁹ W. Carvalho,³ D. Casey,⁴⁵ Z. Casilum,⁵⁰ H. Castilla-Valdez,¹⁷
D. Chakraborty,⁵⁰ K.M. Chan,⁴⁹ S.V. Chekulaev,²¹ D.K. Cho,⁴⁹ S. Choi,²⁸ S. Chopra,⁵¹
B.C. Choudhary,²⁸ J.H. Christenson,³¹ M. Chung,³² D. Claes,⁴⁶ A.R. Clark,²⁴
J. Cochran,²⁸ L. Coney,³⁶ B. Connolly,²⁹ W.E. Cooper,³¹ D. Coppage,³⁸ D. Cullen-Vidal,⁵⁴
M.A.C. Cummings,³³ D. Cutts,⁵⁴ O.I. Dahl,²⁴ K. Davis,²³ K. De,⁵⁵ K. Del Signore,⁴⁴
M. Demarteau,³¹ D. Denisov,³¹ S.P. Denisov,²¹ H.T. Diehl,³¹ M. Diesburg,³¹
G. Di Loreto,⁴⁵ S. Doulas,⁴³ P. Draper,⁵⁵ Y. Ducros,¹² L.V. Dudko,²⁰ S.R. Dugad,¹⁵
A. Dyshkant,²¹ D. Edmunds,⁴⁵ J. Ellison,²⁸ V.D. Elvira,³¹ R. Engelmann,⁵⁰ S. Eno,⁴¹
G. Eppley,⁵⁷ P. Ermolov,²⁰ O.V. Eroshin,²¹ J. Estrada,⁴⁹ H. Evans,⁴⁷ V.N. Evdokimov,²¹
T. Fahland,²⁷ S. Feher,³¹ D. Fein,²³ T. Ferbel,⁴⁹ H.E. Fisk,³¹ Y. Fisyak,⁵¹ E. Flattum,³¹
F. Fleuret,²⁴ M. Fortner,³³ K.C. Frame,⁴⁵ S. Fuess,³¹ E. Gallas,³¹ A.N. Galyaev,²¹
P. Gartung,²⁸ V. Gavrilov,¹⁹ R.J. Genik II,²² K. Genser,³¹ C.E. Gerber,³¹ Y. Gershtein,⁵⁴
B. Gibbard,⁵¹ R. Gilmartin,²⁹ G. Ginther,⁴⁹ B. Gómez,⁵ G. Gómez,⁴¹ P.I. Goncharov,²¹
J.L. González Solís,¹⁷ H. Gordon,⁵¹ L.T. Goss,⁵⁶ K. Gounder,²⁸ A. Goussiou,⁵⁰ N. Graf,⁵¹
P.D. Grannis,⁵⁰ J.A. Green,³⁷ H. Greenlee,³¹ S. Grinstein,¹ P. Grudberg,²⁴ S. Grünendahl,³¹
G. Guglielmo,⁵³ A. Gupta,¹⁵ S.N. Gurzhiev,²¹ G. Gutierrez,³¹ P. Gutierrez,⁵³ N.J. Hadley,⁴¹

H. Haggerty,³¹ S. Hagopian,²⁹ V. Hagopian,²⁹ K.S. Hahn,⁴⁹ R.E. Hall,²⁶ P. Hanlet,⁴³
 S. Hansen,³¹ J.M. Hauptman,³⁷ C. Hays,⁴⁷ C. Hebert,³⁸ D. Hedin,³³ A.P. Heinson,²⁸
 U. Heintz,⁴² T. Heuring,²⁹ R. Hirosky,³² J.D. Hobbs,⁵⁰ B. Hoeneisen,⁸ J.S. Hoftun,⁵⁴
 A.S. Ito,³¹ S.A. Jerger,⁴⁵ R. Jesik,³⁵ T. Joffe-Minor,³⁴ K. Johns,²³ M. Johnson,³¹
 A. Jonckheere,³¹ M. Jones,³⁰ H. Jöstlein,³¹ A. Juste,³¹ S. Kahn,⁵¹ E. Kajfasz,¹⁰
 D. Karmanov,²⁰ D. Karmgard,³⁶ R. Kehoe,³⁶ S.K. Kim,¹⁶ B. Klima,³¹ C. Klopfenstein,²⁵
 B. Knuteson,²⁴ W. Ko,²⁵ J.M. Kohli,¹³ A.V. Kostritskiy,²¹ J. Kotcher,⁵¹ A.V. Kotwal,⁴⁷
 A.V. Kozelov,²¹ E.A. Kozlovsky,²¹ J. Krane,³⁷ M.R. Krishnaswamy,¹⁵ S. Krzywdzinski,³¹
 M. Kubantsev,³⁹ S. Kuleshov,¹⁹ Y. Kulik,⁵⁰ S. Kunori,⁴¹ G. Landsberg,⁵⁴ A. Leflat,²⁰
 F. Lehner,³¹ J. Li,⁵⁵ Q.Z. Li,³¹ J.G.R. Lima,³ D. Lincoln,³¹ S.L. Linn,²⁹ J. Linnemann,⁴⁵
 R. Lipton,³¹ J.G. Lu,⁴ A. Lucotte,⁵⁰ L. Lueking,³¹ C. Lundstedt,⁴⁶ A.K.A. Maciel,³³
 R.J. Madaras,²⁴ V. Manankov,²⁰ S. Mani,²⁵ H.S. Mao,⁴ T. Marshall,³⁵ M.I. Martin,³¹
 R.D. Martin,³² K.M. Mauritz,³⁷ B. May,³⁴ A.A. Mayorov,³⁵ R. McCarthy,⁵⁰ J. McDonald,²⁹
 T. McMahan,⁵² H.L. Melanson,³¹ X.C. Meng,⁴ M. Merkin,²⁰ K.W. Merritt,³¹ C. Miao,⁵⁴
 H. Miettinen,⁵⁷ D. Mihalcea,⁵³ A. Mincer,⁴⁸ C.S. Mishra,³¹ N. Mokhov,³¹ N.K. Mondal,¹⁵
 H.E. Montgomery,³¹ M. Mostafa,¹ H. da Motta,² E. Nagy,¹⁰ F. Nang,²³ M. Narain,⁴²
 V.S. Narasimham,¹⁵ H.A. Neal,⁴⁴ J.P. Negret,⁵ S. Negroni,¹⁰ D. Norman,⁵⁶ L. Oesch,⁴⁴
 V. Oguri,³ B. Olivier,¹¹ N. Oshima,³¹ P. Padley,⁵⁷ L.J. Pan,³⁴ A. Para,³¹ N. Parashar,⁴³
 R. Partridge,⁵⁴ N. Parua,⁹ M. Paterno,⁴⁹ A. Patwa,⁵⁰ B. Pawlik,¹⁸ J. Perkins,⁵⁵
 M. Peters,³⁰ R. Piegaia,¹ H. Piekarczyk,²⁹ B.G. Pope,⁴⁵ E. Popkov,³⁶ H.B. Prosper,²⁹
 S. Protopopescu,⁵¹ J. Qian,⁴⁴ P.Z. Quintas,³¹ R. Raja,³¹ S. Rajagopalan,⁵¹ N.W. Reay,³⁹
 S. Reucroft,⁴³ M. Rijssenbeek,⁵⁰ T. Rockwell,⁴⁵ M. Roco,³¹ P. Rubinov,³¹ R. Ruchti,³⁶
 J. Rutherford,²³ A. Santoro,² L. Sawyer,⁴⁰ R.D. Schamberger,⁵⁰ H. Schellman,³⁴
 A. Schwartzman,¹ J. Sculli,⁴⁸ N. Sen,⁵⁷ E. Shabalina,²⁰ H.C. Shankar,¹⁵ R.K. Shivpuri,¹⁴
 D. Shpakov,⁵⁰ M. Shupe,²³ R.A. Sidwell,³⁹ V. Simak,⁷ H. Singh,²⁸ J.B. Singh,¹³
 V. Sirotenko,³³ P. Slattery,⁴⁹ E. Smith,⁵³ R.P. Smith,³¹ R. Snihur,³⁴ G.R. Snow,⁴⁶
 J. Snow,⁵² S. Snyder,⁵¹ J. Solomon,³² X.F. Song,⁴ V. Sorín,¹ M. Sosebee,⁵⁵ N. Sotnikova,²⁰
 K. Soustruznik,⁶ M. Souza,² N.R. Stanton,³⁹ G. Steinbrück,⁴⁷ R.W. Stephens,⁵⁵

M.L. Stevenson,²⁴ F. Stichelbaut,⁵¹ D. Stoker,²⁷ V. Stolin,¹⁹ D.A. Stoyanova,²¹
M. Strauss,⁵³ K. Streets,⁴⁸ M. Strovink,²⁴ L. Stutte,³¹ A. Sznajder,³ W. Taylor,⁵⁰
S. Tentindo-Repond,²⁹ T.L.T. Thomas,³⁴ J. Thompson,⁴¹ D. Toback,⁴¹ T.G. Trippe,²⁴
A.S. Turcot,⁴⁴ P.M. Tuts,⁴⁷ P. van Gemmeren,³¹ V. Vaniev,²¹ R. Van Kooten,³⁵
N. Varelas,³² A.A. Volkov,²¹ A.P. Vorobiev,²¹ H.D. Wahl,²⁹ H. Wang,³⁴ J. Warchol,³⁶
G. Watts,⁵⁸ M. Wayne,³⁶ H. Weerts,⁴⁵ A. White,⁵⁵ J.T. White,⁵⁶ D. Whiteson,²⁴
J.A. Wightman,³⁷ S. Willis,³³ S.J. Wimpenny,²⁸ J.V.D. Wirjawan,⁵⁶ J. Womersley,³¹
D.R. Wood,⁴³ R. Yamada,³¹ P. Yamin,⁵¹ T. Yasuda,³¹ K. Yip,³¹ S. Youssef,²⁹ J. Yu,³¹
Z. Yu,³⁴ M. Zanabria,⁵ H. Zheng,³⁶ Z. Zhou,³⁷ Z.H. Zhu,⁴⁹ M. Zielinski,⁴⁹ D. Zieminska,³⁵
A. Zieminski,³⁵ V. Zutshi,⁴⁹ E.G. Zverev,²⁰ and A. Zylberstejn¹²

(DØ Collaboration)

¹*Universidad de Buenos Aires, Buenos Aires, Argentina*

²*LAFEX, Centro Brasileiro de Pesquisas Físicas, Rio de Janeiro, Brazil*

³*Universidade do Estado do Rio de Janeiro, Rio de Janeiro, Brazil*

⁴*Institute of High Energy Physics, Beijing, People's Republic of China*

⁵*Universidad de los Andes, Bogotá, Colombia*

⁶*Charles University, Prague, Czech Republic*

⁷*Institute of Physics, Academy of Sciences, Prague, Czech Republic*

⁸*Universidad San Francisco de Quito, Quito, Ecuador*

⁹*Institut des Sciences Nucléaires, IN2P3-CNRS, Université de Grenoble 1, Grenoble, France*

¹⁰*CPPM, IN2P3-CNRS, Université de la Méditerranée, Marseille, France*

¹¹*LPNHE, Universités Paris VI and VII, IN2P3-CNRS, Paris, France*

¹²*DAPNIA/Service de Physique des Particules, CEA, Saclay, France*

¹³*Panjab University, Chandigarh, India*

¹⁴*Delhi University, Delhi, India*

¹⁵*Tata Institute of Fundamental Research, Mumbai, India*

¹⁶*Seoul National University, Seoul, Korea*

- ¹⁷*CINVESTAV, Mexico City, Mexico*
- ¹⁸*Institute of Nuclear Physics, Kraków, Poland*
- ¹⁹*Institute for Theoretical and Experimental Physics, Moscow, Russia*
- ²⁰*Moscow State University, Moscow, Russia*
- ²¹*Institute for High Energy Physics, Protvino, Russia*
- ²²*Lancaster University, Lancaster, United Kingdom*
- ²³*University of Arizona, Tucson, Arizona 85721*
- ²⁴*Lawrence Berkeley National Laboratory and University of California, Berkeley, California 94720*
- ²⁵*University of California, Davis, California 95616*
- ²⁶*California State University, Fresno, California 93740*
- ²⁷*University of California, Irvine, California 92697*
- ²⁸*University of California, Riverside, California 92521*
- ²⁹*Florida State University, Tallahassee, Florida 32306*
- ³⁰*University of Hawaii, Honolulu, Hawaii 96822*
- ³¹*Fermi National Accelerator Laboratory, Batavia, Illinois 60510*
- ³²*University of Illinois at Chicago, Chicago, Illinois 60607*
- ³³*Northern Illinois University, DeKalb, Illinois 60115*
- ³⁴*Northwestern University, Evanston, Illinois 60208*
- ³⁵*Indiana University, Bloomington, Indiana 47405*
- ³⁶*University of Notre Dame, Notre Dame, Indiana 46556*
- ³⁷*Iowa State University, Ames, Iowa 50011*
- ³⁸*University of Kansas, Lawrence, Kansas 66045*
- ³⁹*Kansas State University, Manhattan, Kansas 66506*
- ⁴⁰*Louisiana Tech University, Ruston, Louisiana 71272*
- ⁴¹*University of Maryland, College Park, Maryland 20742*
- ⁴²*Boston University, Boston, Massachusetts 02215*
- ⁴³*Northeastern University, Boston, Massachusetts 02115*
- ⁴⁴*University of Michigan, Ann Arbor, Michigan 48109*

⁴⁵*Michigan State University, East Lansing, Michigan 48824*

⁴⁶*University of Nebraska, Lincoln, Nebraska 68588*

⁴⁷*Columbia University, New York, New York 10027*

⁴⁸*New York University, New York, New York 10003*

⁴⁹*University of Rochester, Rochester, New York 14627*

⁵⁰*State University of New York, Stony Brook, New York 11794*

⁵¹*Brookhaven National Laboratory, Upton, New York 11973*

⁵²*Langston University, Langston, Oklahoma 73050*

⁵³*University of Oklahoma, Norman, Oklahoma 73019*

⁵⁴*Brown University, Providence, Rhode Island 02912*

⁵⁵*University of Texas, Arlington, Texas 76019*

⁵⁶*Texas A&M University, College Station, Texas 77843*

⁵⁷*Rice University, Houston, Texas 77005*

⁵⁸*University of Washington, Seattle, Washington 98195*

Abstract

We present measurements of the $b\bar{b}$ production cross section and angular correlations using the DØ detector at the Fermilab Tevatron $p\bar{p}$ Collider operating at $\sqrt{s} = 1.8$ TeV. The b quark production cross section for $|y^b| < 1.0$ and $p_T^b > 6$ GeV/ c is extracted from single muon and dimuon data samples. The results agree in shape with the next-to-leading order QCD calculation of heavy flavor production but are greater than the central values of these predictions. The angular correlations between b and \bar{b} quarks, measured from the azimuthal opening angle between their decay muons, also agree in shape with the next-to-leading order QCD prediction.

PACS numbers: 13.65.Fy, 12.38.Qk, 13.85.Ni, 13.85.Qk – 14.65.Hq, 13.85.Qk

Measurements of the b quark production cross section and $b\bar{b}$ correlations in $p\bar{p}$ collisions provide an important test of perturbative quantum chromodynamics (QCD) at next-to-leading order (NLO). The measured b quark production cross section at $\sqrt{s} = 1.8$ TeV [1–4] is systematically larger than the central values of the NLO QCD predictions [5,6].

Measurements of $b\bar{b}$ correlations such as the azimuthal opening angle between b and \bar{b} quarks allow additional details of b quark production to be tested since these quantities are sensitive to the relative contributions of different production mechanisms to the total cross section. Two measurements of $b\bar{b}$ angular correlations using the azimuthal opening angle of muons from the heavy quark decays, one at $\sqrt{s} = 1.8$ TeV [7] and another at $\sqrt{s} = 630$ GeV [8], are in qualitative agreement with the NLO QCD predictions. A different measurement at $\sqrt{s} = 1.8$ TeV using the azimuthal opening angle between a muon from B meson decay and the \bar{b} jet shows [4] qualitative differences with the predictions, while a direct measurement [9] of $b\bar{b}$ rapidity correlations is found to be in agreement with the NLO QCD predictions.

In this paper we provide an additional measurement of the b quark production cross section and $b\bar{b}$ angular correlations. The analysis makes use of the fact that the semileptonic decay of a b quark results in a lepton (here a muon) associated with a jet. We use a sample of dimuons and their associated jets to tag both b and \bar{b} quarks. By tagging both the b and \bar{b} quarks, we are able to significantly reduce the number of background events in our data sample. Also included is a revised measurement of the b quark production cross section based on an earlier $D\bar{O}$ analysis [2] using the inclusive single muon measurement.

The $D\bar{O}$ detector and trigger system are described in detail elsewhere [10]. The central muon system consists of three layers of proportional drift tubes and a magnetized iron toroid located between the first two layers. The muon detectors provide a measurement of the muon momentum with a resolution parameterized by $\delta(1/p)/(1/p) = 0.18(p-2)/p \oplus 0.008p$, with p in GeV/ c . The calorimeter is used to measure both the minimum ionizing energy associated with the muon track and the electromagnetic and hadronic activity associated with heavy

quark decay. The total thickness of the calorimeter plus toroid in the central region varies from 13 to 15 interaction lengths, which reduces the hadronic punchthrough in the muon system to less than 0.5% of low transverse momentum muons from all sources. The energy resolution for jets is approximately $80\%/\sqrt{E(\text{GeV})}$.

The data used in this analysis were taken during the 1992–1993 run of the Fermilab Tevatron collider and correspond to a total integrated luminosity $\int \mathcal{L} dt = 6.5 \pm 0.4 \text{ pb}^{-1}$. The dimuon data were collected using a multilevel trigger requiring at least one reconstructed muon with transverse momentum $p_T^\mu > 3 \text{ GeV}/c$ and at least one reconstructed jet with transverse energy $E_T > 10 \text{ GeV}$.

The events are then fully reconstructed offline and subjected to event selection criteria. The offline analysis requires two muons with $p_T^\mu > 4 \text{ GeV}/c$ and pseudorapidity $|\eta^\mu| < 0.8$. In addition, both muon tracks have to be consistent with originating from the reconstructed event vertex and deposit $> 1 \text{ GeV}$ of energy in the calorimeter. Each muon is also required to have an associated jet with $E_T > 12 \text{ GeV}$ within a cone of radius $\mathcal{R} = \sqrt{(\Delta\eta)^2 + (\Delta\phi)^2} < 0.8$. The jet energies are measured using a cone of $\mathcal{R} = 0.7$. Finally, muon candidates in the region $80^\circ < \phi^\mu < 110^\circ$ are excluded due to poor chamber efficiencies near the Main Ring beam pipe.

Further selection criteria are placed on the dimuon candidates to reduce backgrounds to $b\bar{b}$ production. The invariant mass of the dimuons is restricted to the range $6 < m^{\mu\mu} < 35 \text{ GeV}/c^2$. The lower limit removes dimuons resulting from the cascade decay of single b quarks and from J/ψ resonance decays, while the upper limit reduces the number of dimuons due to Z boson decays. An opening space angle requirement of $< 165^\circ$ between the muons is also applied to remove contamination from cosmic ray muons. A total of 397 events pass all selection criteria.

The trigger and offline reconstruction efficiencies are determined from Monte Carlo event samples. Events generated with the ISAJET [11] Monte Carlo are passed through a GEANT [12] simulation of the DØ detector followed by trigger simulation and reconstruction programs. Trigger and some offline efficiencies found in this way are crosschecked by using

appropriate data samples. The overall acceptance times efficiency as a function of the higher (leading) muon p_T in the event increases from about 1% at 4 GeV/ c to a plateau of 9% above 15 GeV/ c . We define the leading muon in the event as the muon with the greater value of p_T^μ .

In addition to $b\bar{b}$ production, dimuon events in the invariant mass range of 6–35 GeV/ c^2 can also arise from other sources. These processes include semileptonic decays of $c\bar{c}$ pairs, events in which one or both of the muons are produced by in-flight decays of π or K mesons, Drell-Yan production, and Υ resonance decays. Muons from the Drell-Yan process and Υ decays are not expected to have jets associated with them. Monte Carlo estimates normalized to the measured Drell-Yan and Υ cross sections [13] show that less than one event is expected to contribute to the final data sample from these two sources. An additional source of dimuon events is cosmic ray muons passing through the detector.

To extract the $b\bar{b}$ signal, we use a maximum likelihood fit with four different input distributions. The input distributions are chosen based on their effectiveness in distinguishing between the different sources of dimuon events. We use the transverse momenta of the leading and trailing muons relative to their associated jet axes (p_T^{rel}), the fraction of longitudinal momentum of the jet carried by the leading muon divided by the jet E_T (r_z), and the reconstructed time of passage (t_0) of the leading muon track through the muon chambers with respect to the beam crossing time. The variable t_0 is used to identify the cosmic ray muon background, which is not expected to be in time with the beam crossing. Monte Carlo studies show that the variables p_T^{rel} and r_z help to discriminate between background and $b\bar{b}$ production. For both variables, the jet energy is defined to be the vector sum of the muon energy and the jet energy measured in the calorimeter less the expected minimum ionizing energy of the muon deposited in the calorimeter.

The p_T^{rel} and r_z distributions for $b\bar{b}$, $c\bar{c}$, and b or c plus π/K decay are modeled using the ISAJET Monte Carlo. Each of these samples is processed with a complete detector, trigger, and offline simulation. The distributions for b quark decays includes both direct ($b \rightarrow \mu$) and sequential ($b \rightarrow c \rightarrow \mu$) decays. The distributions for $c\bar{c}$ and a c quark plus

a π or K decay are very similar, so both contributions are fit to the same function. The distributions for t_0 are obtained from two different sources. The t_0 distribution for cosmic ray muons is obtained from data collected between collider runs using cosmic ray triggers. For beam-produced muons, t_0 is measured using muons from J/ψ decays.

Figure 1 shows the result of the maximum likelihood fit for p_T^{rel} of the leading muon and r_z . Included in Fig. 1 are the contributions from each of the major sources of dimuon events. The $b\bar{b}$ contribution to the final data sample is found to be $45.3\pm 5.8\%$. The other fractions fit to the data set consist of b quark plus π/K decay ($37.9\pm 5.6\%$), $c\bar{c}$ production ($14.0\pm 3.8\%$), and cosmic ray muons ($2.8\pm 1.6\%$). From the fit, we obtain the number of $b\bar{b}$ events per bin as a function of p_T^μ of the leading muon and as a function of the difference in azimuthal angle between the two muons, $\Delta\phi^{\mu\mu}$.

The systematic errors on the number of $b\bar{b}$ events per bin (8%) are estimated by varying the input distributions to the maximum likelihood fit within reasonable bounds. As a crosscheck of the fitting procedure, we calculate the fraction of events originating from $b\bar{b}$ production using appropriately normalized Monte Carlo samples. Good agreement is found between the Monte Carlo calculated fraction and that found from the maximum likelihood fit to the data. The fractions agree as a function of both p_T of the leading muon and $\Delta\phi^{\mu\mu}$. A complete description of the fitting procedure can be found in Ref. [14].

The dimuon cross section originating from $b\bar{b}$ production is calculated using

$$\frac{d\sigma_{b\bar{b}}^{\mu\mu}}{dx} = \frac{1}{\Delta x} \frac{N_{b\bar{b}}^{\mu\mu}(x) f_p(x)}{\epsilon(x) \int \mathcal{L} dt}, \quad (1)$$

where x is either the p_T of the leading muon or $\Delta\phi^{\mu\mu}$. Here, ϵ is the total efficiency, $\int \mathcal{L} dt$ is the integrated luminosity, $N_{b\bar{b}}^{\mu\mu}$ is the number of $b\bar{b}$ events determined from the fit, and f_p is an unfolding factor to account for smearing caused by the muon momentum resolution. An unfolding technique [15] is used to determine f_p . The factor f_p varies from 0.78 at low $p_T^{\mu_1}$ to 0.93 in the highest $p_T^{\mu_1}$ bin (μ_1 is the leading muon in the event) and takes into account our invariant mass and p_T^μ requirements. The systematic uncertainty associated with f_p is found to be p_T^μ dependent and varies from 13% to 22%.

Figure 2(a) shows the result of the cross section calculation as a function of $p_T^{\mu_1}$ for $4 < p_T^\mu < 25$ GeV/ c , $|\eta^\mu| < 0.8$, and $6 < m^{\mu\mu} < 35$ GeV/ c^2 . The total systematic error is found to be $p_T^{\mu_1}$ dependent, ranging from 25% to 31%. This includes uncertainties from the trigger efficiency (19%), offline selection efficiency (5%), maximum likelihood fit (8%), momentum unfolding (13–22%), and integrated luminosity (5%).

The theoretical curve of Fig. 2(a) is determined using the HVQJET [16] Monte Carlo. HVQJET is an implementation of the NLO calculation of Ref. [6] (MNR) for $b\bar{b}$ production. It uses the MNR parton level generator and a modified version of ISAJET for hadronization, particle decays, and modeling of the underlying event. The particle decays are based on the ISAJET implementation [17] of the CLEO decay tables. In HVQJET the MNR prediction is realized by combining parton level events having negative weights with those having positive weights and similar topologies. The prediction shown is the NLO calculation and includes all four gg , gq , $g\bar{q}$, and $q\bar{q}$ initiated subprocesses with $m_b(\text{pole mass}) = 4.75$ GeV/ c^2 . The MRSR2 [18] parton distribution functions (PDFs) are used with $\Lambda_5 = 237$ MeV.

The shaded region in Fig. 2(a) shows the combined systematic and statistical error from the HVQJET prediction ($^{+74}_{-50}\%$). This error is dominated by the uncertainty associated with the MNR prediction and is determined by varying the mass of the b quark between 4.5 GeV/ c^2 and 5.0 GeV/ c^2 , and the factorization and renormalization scales, taken to be equal, between $\mu_0/2$ and $2\mu_0$, where $\mu_0^2 = m_b^2 + \langle p_T^b \rangle^2$. Additional systematic errors include those associated with the PDFs (20%), the Peterson fragmentation function [19] (8%), the B meson semileptonic branching fraction (7%), and the muon decay spectrum from B mesons (20%). Varying these parameters does not appreciably change the shape of the prediction. The Monte Carlo statistical errors are less than 10%.

To extract the b quark cross section from the dimuon data, we employ a method first used by UA1 [20] and subsequently used by CDF [1] and DØ [2]. Since a correlation exists between the p_T of the muon produced in a b quark decay and the parent b quark p_T , cuts applied to the muon p_T in the data are effectively b quark p_T cuts. For a set of kinematic cuts, which include cuts on the transverse momentum of the muons, we define p_T^{min} as that

value of the b quark p_T where 90% of the accepted events have b quark transverse momentum greater than p_T^{\min} . The b quark cross section is then calculated as

$$\sigma_b(p_T^b > p_T^{\min}) = \sigma_{bb}^{\mu\mu}(p_T^{\mu_1}) \frac{\sigma_b^{\text{MC}}}{\sigma_{bb \rightarrow \mu\mu}^{\text{MC}}}, \quad (2)$$

where $\sigma_{bb}^{\mu\mu}(p_T^{\mu_1})$ is the measured dimuon cross section of Eq. (1) integrated over different intervals of $p_T^{\mu_1}$, σ_b^{MC} is the total Monte Carlo b quark cross section for $p_T^b > p_T^{\min}$ (where $|y^b| < 1.0$ and no cut on $y^{\bar{b}}$), and $\sigma_{bb \rightarrow \mu\mu}^{\text{MC}}$ is the Monte Carlo cross section for dimuon production with the same requirements used to select the data set. For each interval of $p_T^{\mu_1}$, p_T^{\min} and σ^{MC} are calculated using HVQJET. Combining the uncertainties of the measured dimuon cross section with those associated with extracting the b quark cross section, we obtain a total systematic uncertainty of 34–38% on the measured b quark cross section. The latter uncertainties are associated with b quark fragmentation: Peterson fragmentation function; semileptonic branching fraction; and muon decay spectrum with the magnitudes noted above.

Figure 2(b) shows the b quark production cross section for the rapidity range $|y^b| < 1.0$ as a function of p_T^{\min} . The NLO QCD prediction is computed using Ref. [6] with $m_b(\text{pole mass}) = 4.75 \text{ GeV}/c^2$ and the MRSR2 PDFs. The theoretical uncertainty of $^{+47\%}_{-28\%}$ results from varying the mass of the b quark and the factorization and renormalization scales as described above and is dominated by the variation of the scales. The ratio of the data to the central NLO QCD prediction is approximately three over the entire p_T^{\min} range covered.

Also shown in Fig. 2(b) is a revised result based on the previous inclusive single muon measurement from $D\bar{O}$ [2]. In light of revised B meson decay modes and Monte Carlo improvements, the cross section is re-evaluated by using HVQJET to calculate new values of $\sigma_b^{\text{MC}}/\sigma_{b \rightarrow \mu}^{\text{MC}}$ for extraction of the b quark cross section from the measured inclusive single muon spectrum. In addition, the high p_T inclusive muon data ($p_T^\mu > 12 \text{ GeV}/c$) are excluded due to large uncertainties in the cosmic ray muon background subtractions. The resulting increase in the b quark cross section is primarily caused by the new B meson decay modes and lower semileptonic branching fractions [17]. The re-evaluated cross section supersedes

that of Ref. [2]. The tabulated data for the dimuon and inclusive single muon data sets can be found in Tables I and II.

The differential $b\bar{b}$ cross section, $d\sigma_{b\bar{b}}^{\mu\mu}/d\Delta\phi^{\mu\mu}$, gives further information on the underlying QCD production mechanisms. The azimuthal opening angle between b and \bar{b} quarks (or between their decay muons) is sensitive to the contributing production mechanisms. These contributions are the leading order (LO) subprocess, flavor creation, and the next-to-leading order subprocesses, gluon splitting and flavor excitation. There are also contributions from interference terms.

The cross section $d\sigma_{b\bar{b}}^{\mu\mu}/d\Delta\phi^{\mu\mu}$ is shown in Fig. 3. Also shown are the LO and NLO QCD predictions which are determined using HVQJET and include all subprocesses. The grey band around the NLO prediction shows the combined statistical and systematic errors associated with the prediction, which is ${}^{+74}_{-50}\%$ as detailed above. The data again show an excess above the NLO QCD prediction but agree with the overall shape. The agreement in shape is consistent with the presence of NLO subprocesses since the LO prediction, which contains the smearing from the $b \rightarrow B \rightarrow \mu$ fragmentation and decay chain, does not describe the data.

In conclusion, we have measured the b quark production cross section and the $b\bar{b}$ azimuthal angle correlations using dimuons to tag the presence of b quarks. These measurements, as well as the revised inclusive single muon measurement, are found to agree in shape with the NLO QCD calculation of heavy flavor production but lie above the central values of these predictions.

We thank the staffs at Fermilab and at collaborating institutions for contributions to this work, and acknowledge support from the Department of Energy and National Science Foundation (USA), Commissariat à L'Énergie Atomique and CNRS/Institut National de Physique Nucléaire et de Physique des Particules (France), Ministry for Science and Technology and Ministry for Atomic Energy (Russia), CAPES and CNPq (Brazil), Departments of Atomic Energy and Science and Education (India), Colciencias (Colombia), CONACyT (Mexico), Ministry of Education and KOSEF (Korea), CONICET and UBACyT

(Argentina), A.P. Sloan Foundation, and the Humboldt Foundation.

REFERENCES

- [1] CDF Collaboration, F. Abe *et al.*, Phys. Rev. Lett. **71**, 2396 (1993).
- [2] DØ Collaboration, S. Abachi *et al.*, Phys. Rev. Lett. **74**, 3548 (1995).
- [3] DØ Collaboration, S. Abachi *et al.*, Phys. Lett. B **370**, 239 (1996).
- [4] CDF Collaboration, F. Abe *et al.*, Phys. Rev. D **53**, 1051 (1996).
- [5] P. Nason, S. Dawson, and R.K. Ellis, Nucl. Phys. **B327**, 49 (1989).
- [6] M. Mangano, P. Nason, and G. Ridolfi, Nucl. Phys. **B373**, 295 (1992).
- [7] CDF Collaboration, F. Abe *et al.*, Phys. Rev. D **55**, 2546 (1997).
- [8] UA1 Collaboration, C. Albajar *et al.*, Z. Phys. **C 61**, 41 (1994).
- [9] CDF Collaboration, F. Abe *et al.*, Phys. Rev. D **61**, 032001 (2000).
- [10] DØ Collaboration, S. Abachi *et al.*, Nucl. Instrum. Methods Phys. Res. A **338**, 185 (1994).
- [11] F. Paige and S. Protopopescu, BNL Report No. BNL38034, 1986 (unpublished).
- [12] F. Carminati *et al.*, “GEANT Users Guide”, v 3.15, CERN Program Library, December, 1991 (unpublished).
- [13] A. Smith, Ph.D. Thesis, University of Arizona, 1996 (unpublished), http://www-d0.fnal.gov/results/publications_talks/thesis/smith/thesis.ps.
CDF Collaboration, F. Abe *et al.*, Phys. Rev. Lett. **75**, 4358 (1995), Phys. Rev. D **50**, R1 (1994).
- [14] D. Fein, Ph.D. Thesis, University of Arizona, 1996 (unpublished), http://www-d0.fnal.gov/results/publications_talks/thesis/fein/df_thesis.ps.
- [15] G. D’Agostini, DESY Report No. 94-099, 1994.

- [16] M. Baarmand and F. Paige, HVQJET Monte Carlo Event Generator, private communication.
- [17] Particle decays based on the CLEO decay tables are implemented in ISAJET starting with V7.22.
- [18] A. Martin, R. Roberts, and W.J. Stirling, Phys. Lett. B **387**, 419 (1996).
- [19] C. Peterson *et al.*, Phys. Rev. D **27**, 105 (1983).
- [20] UA1 Collaboration, C. Albajar *et al.*, Phys. Lett. B **256**, 121 (1991).

FIGURE CAPTIONS

Figure 1 The results of the maximum likelihood fit to the data for (a) p_T^{rel} of the leading muon and (b) r_z . Also included are the curves showing the contribution from each process to the dimuon sample.

Figure 2 (a) The unfolded leading muon p_T spectrum for $b\bar{b}$ production compared to the predicted spectrum (see text) where the data errors are statistical (inner) and total (outer) and the Monte Carlo errors are total (shaded band); (b) the b quark production cross section for $|y^b| < 1.0$ compared with the revised inclusive single muon results and the NLO QCD prediction. The error bars on the data represent the total error. The theoretical uncertainty shows the uncertainty associated with the factorization and renormalization scales and the b quark mass. Also shown are the inclusive single muon data from CDF [1].

Figure 3 The $\Delta\phi^{\mu\mu}$ spectrum for $b\bar{b}$ production compared to the predicted spectrum (see text). The errors on the data are statistical and total. The solid histogram shows the NLO prediction with the grey band indicating the total uncertainty. Also shown is the LO prediction (dotted histogram) with the statistical error only.

FIGURES

Figure 1

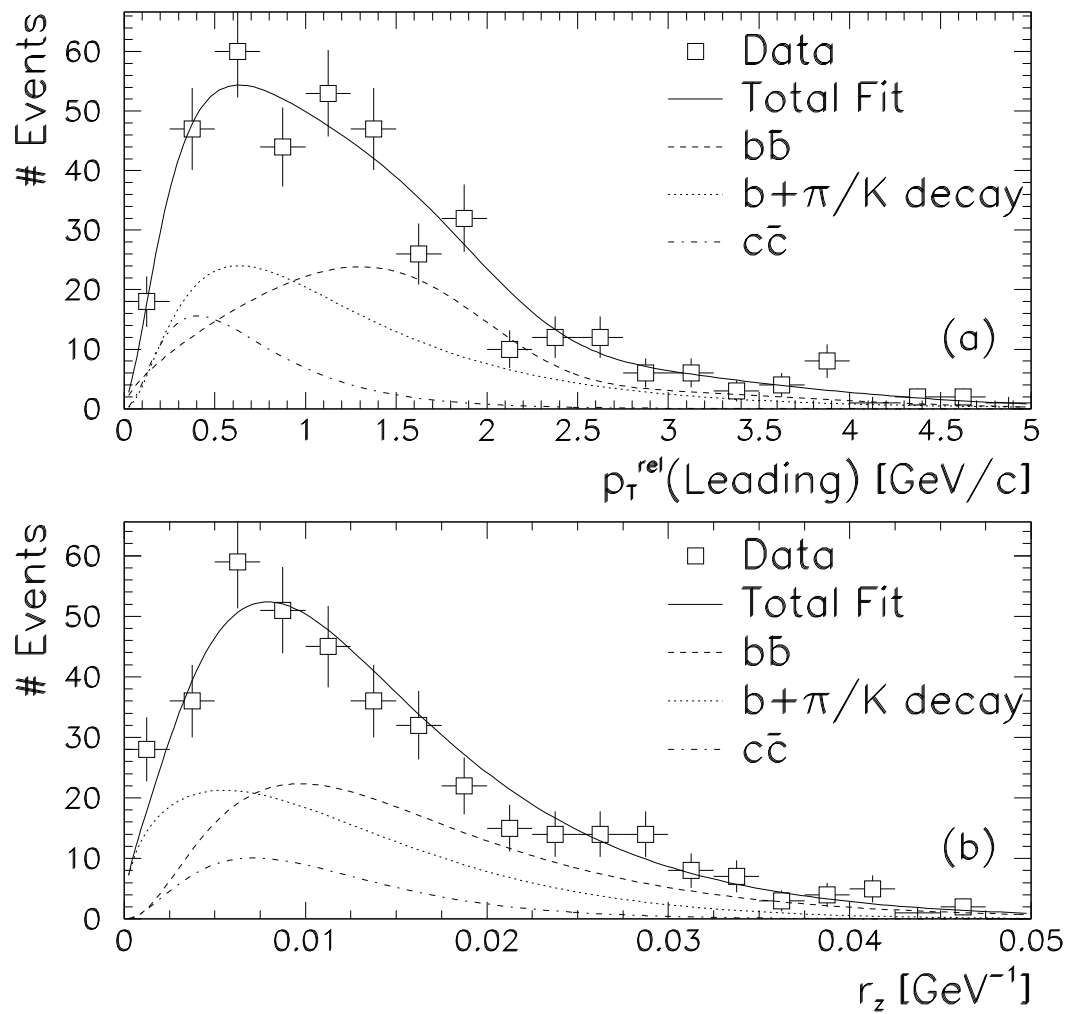


Figure 2

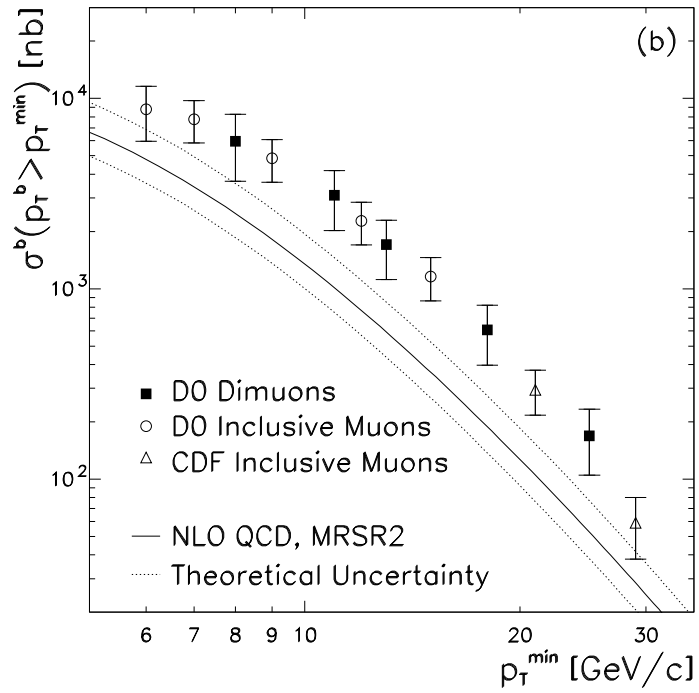
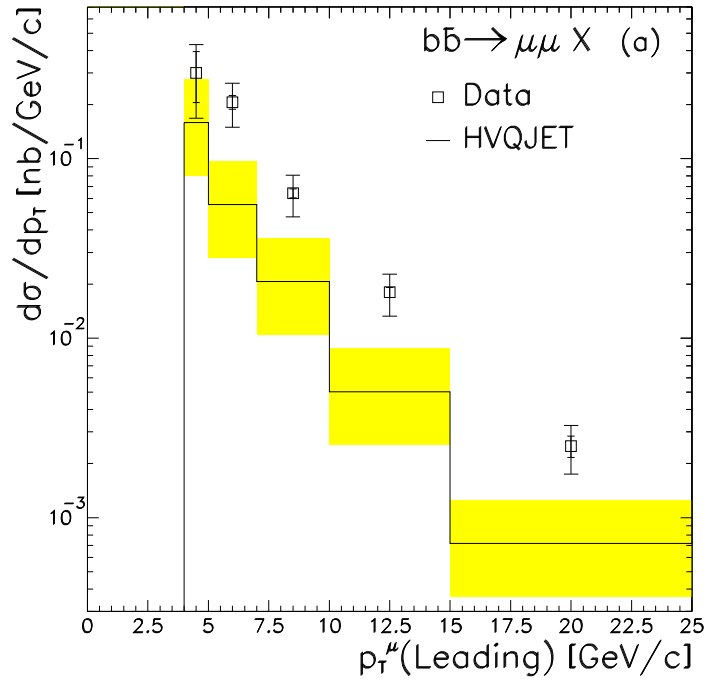


Figure 3

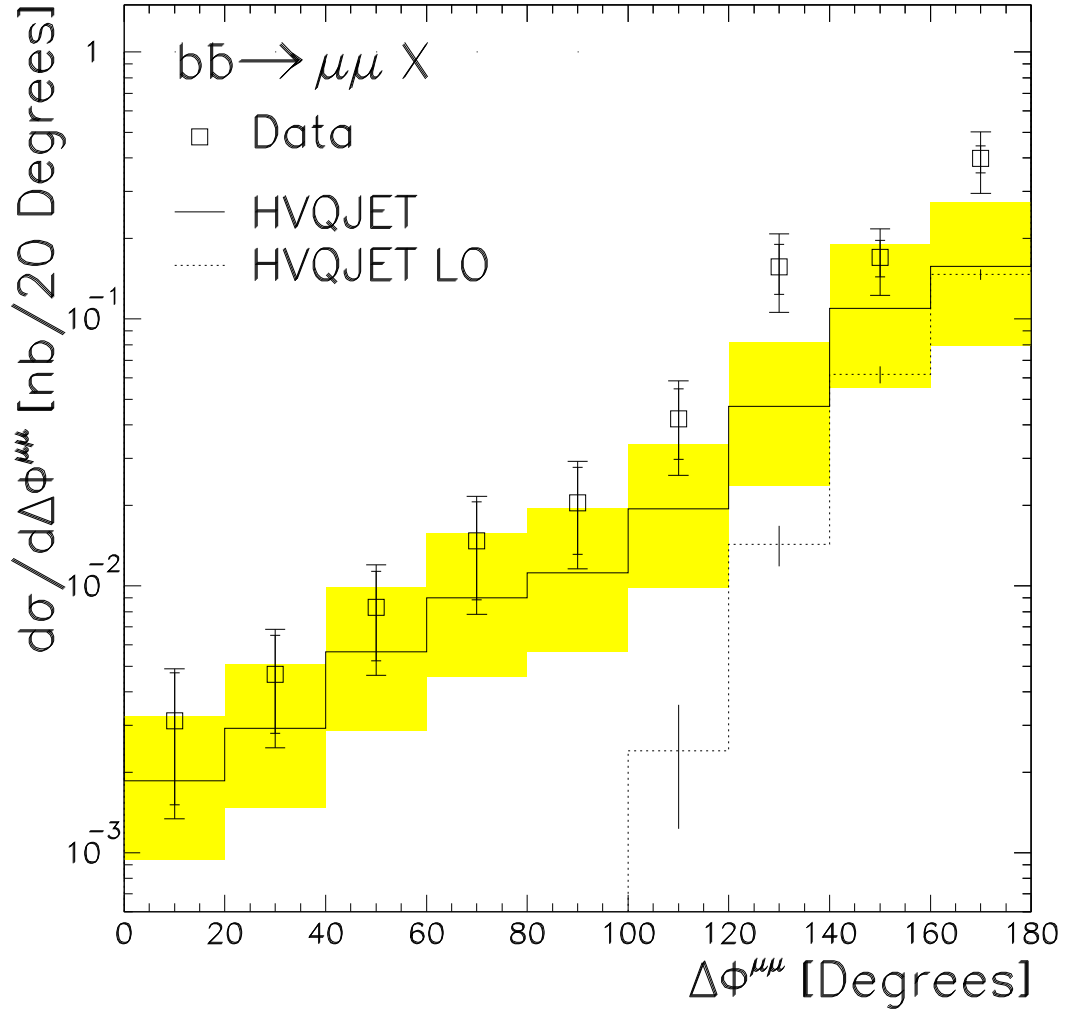


TABLE CAPTIONS

Table 1 Cross sections for $b\bar{b} \rightarrow \mu\mu$ production.

Table 2 Results for the b quark production cross section for $|y^b| < 1.0$.

TABLES

Table 1

$p_T^{\mu 1}$	$d\sigma^{\mu\mu}/dp_T$	Stat Error	Syst Error
[GeV/c]	[nb/GeV/c]	[nb/GeV/c]	[nb/GeV/c]
4-5	0.30	0.095	0.092
5-7	0.21	0.018	0.054
7-10	0.064	0.0037	0.016
10-15	0.018	0.0012	0.0046
15-25	0.0025	0.00034	0.00067

Table 2

p_T^b [GeV/c]	σ^b [μb]	Total Error [μb]	Data Source
6	8.76	2.80	Single Muon
7	7.78	1.95	Single Muon
8	5.96	2.29	Dimuon
9	4.85	1.22	Single Muon
11	3.10	1.08	Dimuon
12	2.28	0.58	Single Muon
13	1.71	0.59	Dimuon
15	1.16	0.30	Single Muon
18	0.61	0.21	Dimuon
25	0.17	0.06	Dimuon